Structural, electronic, magnetic and calorimetric study of the metal-insulator transition in $NdNiO_{3-delta}$

1994 J. Phys.: Condens. Matter 6 5875

(http://iopscience.iop.org/0953-8984/6/30/009)

J. Phys.: Condens. Matter 6 (1994) 5875–5889. Printed in the UK

Structural, electronic, magnetic and calorimetric study of the metal–insulator transition in $NdNiO_{3-\delta}$

J Blasco, M Castro and J García

Instituto de Ciencia de Materiales de Aragón, Consejo Superior de Investigaciònes Científicas–Universidad de Zaragoza, Facultad de Ciencias, Plaza San Francisco s/n, 50009 Zaragoza, Spain

Received 5 January 1994, in final form 18 April 1994

Abstract. $NdNiO_3$ has been prepared using a low-temperature low-oxygen-pressure method. This compound has the same crystallographic structure as its homologous $NdNiO_3$ synthesized at high oxygen pressures. The sample obtained shows a metal–insulator transition at around 205 K with a large thermal hysteresis. The metallic phase shows a linear resistivity temperature dependence while, at low temperatures, conduction by variable-range hopping is observed. The heat capacity, magnetic susceptibility and electrical resistivity indicate carrier spin correlation even in the high-temperature metallic phase.

1. Introduction

Mixed rare-earth nickel oxides are being investigated with renewed interest in recent years [1–4]. This is related to the discovery of high-temperature superconductivity in the perovskite-like copper oxides that have enhanced the efforts to understand the electronic properties of related oxides. These oxides belong to a more extensive group of transition-metal compounds in which the interpretations of the magnetic and transport properties have been controversial topics over the last 40 years [5]. The $RENiO_3$ perovskites which present a metal–insulator transition by changing the temperature (RE ≡ Pr, Nd, Sm or Eu) are a most interesting case. These compounds have been described as a charge-transfer type, the transition originating from the closing–opening of the charge-transfer gap [6].

It is well known that the physical properties depend on the chosen preparation procedure. In particular, $NdNiO_3$ has been synthesized by two different methods:

(i) sintering the mixture of binary oxides at a high oxygen pressure and a high temperature (hereafter denoted HT-$NdNiO_3$) [1–4] and

(ii) sintering at a low oxygen pressure (p_{O_2} = 1 atm) and a low temperature (923 K) by means of a sol–gel method [7, 8].

Samples synthesized using the first method have been exhaustively studied in recent years [1–4, 6, 9, 10]. They show a perovskite-type unit cell orthorhombically distorted with the $GdFeO_3$ structure [1]. These samples have a metal–insulator transition at around 200 K and it has been described by the appearance of magnetic ordering at the temperature of the metal–insulator transition with the formation of a spin-density wave [11]. Moreover, reasonable doubt exists about the electronic charge of the Ni atom in these oxides, although neutron diffraction experiments indicate that the Ni atom is in the low-spin Ni(III) state [1, 11]. This result is in contrast with the strong evidence for holes in the oxygen band

0953-8984/94/305875+15$19.50

in $RENiO_3$ (RE≡La, Pr or Nd) [12] and in several doped and non-stoichiometric nickel oxides ($Ni_{1-x}Li_xO_2$) [13]. On the other hand, in $NdNiO_3$, x-ray absorption experiments no chemical shift at the Ni K edge has been observed [14].

Surprisingly few studies have been reported on samples prepared using the easier second method [7]. Recently, we discovered that samples sintered at low temperatures crystallize in an orthorhombic unit cell like HT-$NdNiO_3$ [8] and are not rhombohedral as previously reported [7].

In this work we have paid attention to two important aspects of $NdNiO_3$ prepared by the second method. The first is related to possible differences in the microstructures due to the sintering procedure. The second important topic deals with a detailed phenomenological characterization of the metal–insulator transition and its correlation with the nickel sublattice magnetism. With this aim, measurements of the electrical resistivity, magnetic susceptibility, magnetization and heat capacity as functions of temperature were performed.

We shall show that samples prepared at low oxygen pressures have the same crystallographic structure as HT-$NdNiO_3$. Differences in preparation method are mainly connected to the grain size of the material. On the other hand, the analysis of $\rho(T)$ shows that conduction at low temperatures occurs by variable-range hopping (VRH). Moreover, magnetic and calorimetric studies show some magnetic ordering at the metal–insulator transition but it is far from classical ordering of localized magnetic moments. All these results will be discussed considering the polaron formation hypothesis.

2. Experimental section

2.1. Preparation

The samples were prepared by the sol–gel method described elsewhere [7, 8], mixing the Nd^{3+} and Ni^{2+} solution in the appropriate stoichiometry with citric acid and ethylene glycol. A green gel was obtained by heating the resultant solution. The gel was fired to give a brown powder precursor which was calcined at 673 K under an oxygen current flow overnight. The resulting powder was pressed to 4 kbar and the pellets were sintered for 10 d at 923 K in an oxygen current flow with several grindings. In order to characterize the sintering process, several samples were removed at intermediate sintering times of 1 d (sample d) and 5 d (sample c). The pellets obtained after sintering for 10 d are identified as samples b. Finally, several samples b were ground, repelleted and sintered at 1023 K in the same oxygen atmosphere for 1 d (samples a).

2.2. Characterization

All pellets prepared were black and not very hard and had a high electrical conductivity at room temperature. The density calculated using the Archimedes method for these samples was around 60–70% of the theoretical value [8]. They are single phase as inferred from their x-ray patterns. The x-ray diffraction patterns were obtained at room temperature with a Rigaku D-max system using Cu Kα radiation from a rotating anode. A graphite monochromator was used in reflected light.

The Ni and Nd contents were determined by fluorescence analysis using a JEOL JSM-6400 electronic microscope and a Link Analytical EDS x-ray spectrometer. The analysed volume was 1–2 μm^3 and several zones were selected in each sample to perform a correct analysis. The Nd:Ni atomic ratio was 1 for all the samples.

The oxygen content of the samples was found by thermogravimetric analysis (TGA) using a Perkin–Elmer TG-S2 system. A nominal composition of $NdNiO_{2.91\pm0.03}$ was obtained for

all the samples, indicating that the $NdNiO_3$ synthesized by this sol–gel method is an oxygen-deficient phase.

Resistivity and magnetic susceptibility measurements as functions of the temperature were performed in a temperature-controlled multipurpose cryostat from 4.2 to 300 K. The resistivity of bars with 1.5 mm × 1.5 mm × 5.5 mm dimensions, cut from the pellets, were measured using a four-probe AC (ν = 20 Hz) method. AC magnetic susceptibility measurements of the samples were made from 1.7 to 300 K by the determination of the magnetic flux variation on a pick-up coil system [15]. The determination of DC magnetization was carried out using the same pick-up coil system and a superconducting coil generating the external DC magnetic field. The intensity of the DC field can reach 5 T as a maximum value.

Heat capacity measurements from 4 to 300 K were carried out on a commercial AC calorimeter from Sinku-Riko Company (model ACC-IVL, Sinku-Rico Ltd, Japan). A slab-shaped sample of pressed powder of around 3 mg mass and 0.3 mm thick was used in the experiment. The selected frequency for the heating power was 1.5 Hz. Absolute values were obtained by scaling the relative values to the absolute heat capacity at room temperature measured in a Perkin–Elmer DSC7 instrument. The heat capacity of $NdNiO_3$ was recorded in a heating run from 4 K to room temperature and a cooling run from room temperature to 77 K. The heat capacity of $NdGaO_3$ (as the reference sample) was also measured in the same temperature range.

3. Results

3.1. Structure

The x-ray diffraction patterns of the precursor powder (sample e) and the different samples (a–d) prepared are shown in figure 1. The precursor pattern does not show any diffraction peaks, indicating the amorphous character of the powder and confirming the intimate mixture of the components in the starting material. The other patterns show characteristic diffraction peaks of a perovskite phase. The peak broadening, which decreases with increasing sintering time, indicates a small grain size for all the samples. The average grain size of each sample has been estimated from the analysis of the diffraction peak width by means of the Scherrer equation using an internal standard. The grain size obtained was 100 Å for samples d, 165 Å for samples c, 325 Å for samples b and 410 Å for samples a.

The x-ray patterns of most crystallized samples (a and b) clearly show low-intensity peaks (indicated by asterisks in figure 1), which is characteristic of the orthorhombic distortion of the perovskite phase. Therefore this result demonstrates that $NdNiO_3$ synthesized using a sol–gel method crystallizes in the same structure as samples sintered at high oxygen pressures. The lattice parameters obtained for sample a and that reported for HT-$NdNiO_3$ samples are compared in table 1. The unit cells for these samples are very similar and the only difference is the orthorhombic strain defined as $s = 2(a - b)/(a + b)$, higher for the sample sintered at a low oxygen pressure, indicating slightly larger orthorhombic distortion of the unit cell.

We have analysed the high-resolution pattern using the Rietveld method with the aid of the FULLPROFF code [16]. The best fit achieved corresponds to an orthorhombic cell, of space group *Pbnm*. The structural results obtained are close to the HT-$NdNiO_3$ data [1] showing that no crystallographic differences exist from the material prepared at high oxygen pressures. In spite of this result, the agreement is not completely satisfactory because of the presence of an anomalous asymmetric shape of some diffraction peaks. It indicates the

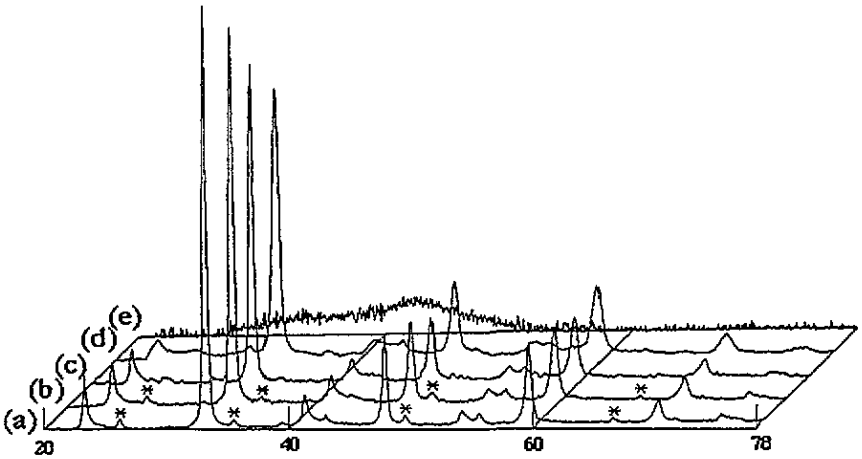

Figure 1. X-ray diffraction patterns of sample a sintered for 10 d at 923 K and 1 d at 1023 K; (curve (a)), sample b sintered for 10 d at 923 K; (curve (b)), sample c sintered for 5 d at 923 K; (curve (c)) sample d sintered for 1 d at 923 K; (curve (d)) and powder precursor, i.e. sample e (curve (e)).

Table 1. Room-temperature x-ray parameters of sol–gel $NdNiO_{3-\delta}$ sample, compared with reported HT-$NdNiO_3$ values (s is the orthorhombic strain).

	Sol–gel $NdNiO_{3-\delta}$	HT-$NdNiO_3$		
a (Å)	5.401	5.384	5.388	5.3891
b (Å)	5.377	5.384	5.3845	5.3816
c (Å)	7.609	7.615	7.6127	7.6101
Volume (Å^3)	220.98	220.74	220.86	220.71
s (10^{-3})	4.4	—	0.65	1.4
Reference	This work	[4]	[2]	[1]

existence of dislocations or imperfections that are characteristic of some laminar disorder in its structure [17]. Indexing the main reflections of the diffraction pattern in the pseudocubic cell, this anomalous broadening occurs systematically in reflections with $h+k+l=2n$, while the symmetric peaks are those with $h+k+l=2n+1$. A possible explanation of this behaviour might be the existence of a dislocation of the planes (111) of the pseudocubic cell. The lack of oxygen stoichiometry (i.e. the presence of oxygen vacancies) of these samples could be reponsible for this laminar disorder. In order to check this hypothesis, we plan to perform a structural study by means of transmission electron microscopy.

The determination of the local structure around the Ni atom for the samples poorly crystallized (samples c and d) by means of EXAFS at the Ni K edge have confirmed the same orthorhombic structure for these samples [8].

3.2. Electrical properties

The electrical resistivity measurements from 4 to 300 K of sample a for different heating and cooling cycles are shown in figure 2. The sharp discontinuity in the heating curve at 205 K indicates the insulator–metal transition. The temperature of this phase transition is very close to that reported for HT-$NdNiO_3$ by other workers [1, 2, 4]. The second point to be stressed is the different behaviour of the cooling resistivity curve. As observed in figure 2,

when the sample is heated from 4.2 to 300 K, the resistivity follows curve a, showing a sharp $d\rho/dT$ discontinuity at 205 K. When the sample is cooled from room temperature, the resistivity leaves curve a at 205 K and follows curve b. This curve joins curve a again at 15 K, as can be seen in figure 2. This experiment shows the large hysteresis behaviour of this phase transition. This effect has been checked several times changing either the heating and cooling rates or the current intensity across the sample (from 0.1 to 10 mA).

This behaviour is similar to that reported for HT-$NdNiO_3$ but two differences are noted. First, the thermal hysteresis is larger for the sample synthesized at a low oxygen pressure [7]. Second, the metal–insulator transition when the sample is cooled from 300 K is less sharp than when the sample is heated from 4.2 K while HT-$NdNiO_3$ shows the same discontinuity in both conditions [9].

In order to characterize the hysteresis behaviour we have performed several runs in different conditions. When the sample is heated from 4.2 K to a temperature lower than 205 K and the sample is cooled again, the resistivity curve always follows the same curve a. Nevertheless, if the sample is cooled to a temperature below the minimum resistivity (180 K) and heated again, the resistivity does not follow curve b and new hysteresis cycles appear. Resistivity curves in heating runs obtained after cooling to 77 K and 120 K (curves c and d, respectively) are shown in figure 2. This result shows the continuous transformation of the high-temperature phase to the low-temperature phase and the two phases coexist over a large temperature range. In this case, the metallic phase would be metastable. This type of metastable phase has been reported recently in related compounds and similar hysteresis cycles have been obtained in resistance and Seebeck effect measurements on HT-$NdNiO_3$ and HT-$PrNiO_3$ [10]. In order to study its stability, resistivity measurements as a function of time were performed on samples cooled to 77 K from room temperature. After 1 d, the resistivity increase of the sample was only around 1.5% of the increase estimated for the full conversion of the metallic phase to the insulator phase. This result indicates the slow phase transformation for this system at this temperature.

Resistivity measurements of samples b–d reported in figure 3 show the same behaviour. Some differences according to the grain size of the sample are observed. Higher absolute resistance values of the metallic phase are observed for samples with a lower grain size. These differences may be related to the different grain boundary contributions to the resistivity. All samples show the same transition temperature and similar thermal hysteresis, indicating that these properties do not depend on the grain size.

We have analysed the resistivity dependence as a function of temperature in the two phases. The $\ln \rho$ versus $1000/T$ data obtained by heating sample a from 4.2 K to the metal–semiconductor transition is shown in figure 4. The curve is far from a straight line, presenting a continuous curvature with a striking change in slope at around 60–80 K. This result implies that the activation energy E_a is highly temperature dependent. At low temperatures ($T = 4.2$ K), E_a is close to 1 K while it takes the value of 990 K at temperatures below the phase transition. This value is an approximate estimation of the semiconducting gap. The shape of the curve is in agreement with previous work for this system [7], although our E_a are slightly lower. Small differences may be related to the fact that, in that work, the activation energies were obtained using the cooling curve (similar to curve b in figure 2) and, as has been demonstrated, this curve corresponds to the resistivity of a mixture of two phases (metallic and insulating).

The behaviour of the resistivity (see figure 4) resembles closely that reported for NiO doped with lithium [17, 18]. For this system, the electrical transport properties at low temperatures have been explained in terms of either the impurity conduction mechanism [17] or polaron formation [19]. Following the suggestion of Mott [19], the experimental

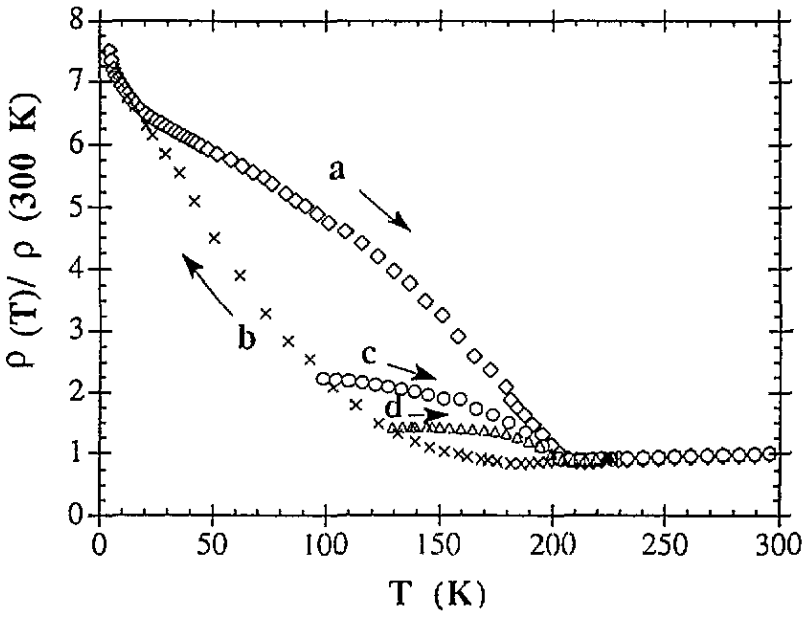

Figure 2. Resistivity of sample a measured under the following conditions: data a, ◊, heating from 4.2 K on the sample previously cooled to 4.2 K; data b, ×, cooling the sample from 300 to 4.2 K; data c, ○, heating from 77 K on the sample cooled to 77 K previously; data d, △, heating from 120 K on the sample cooled to 120 K.

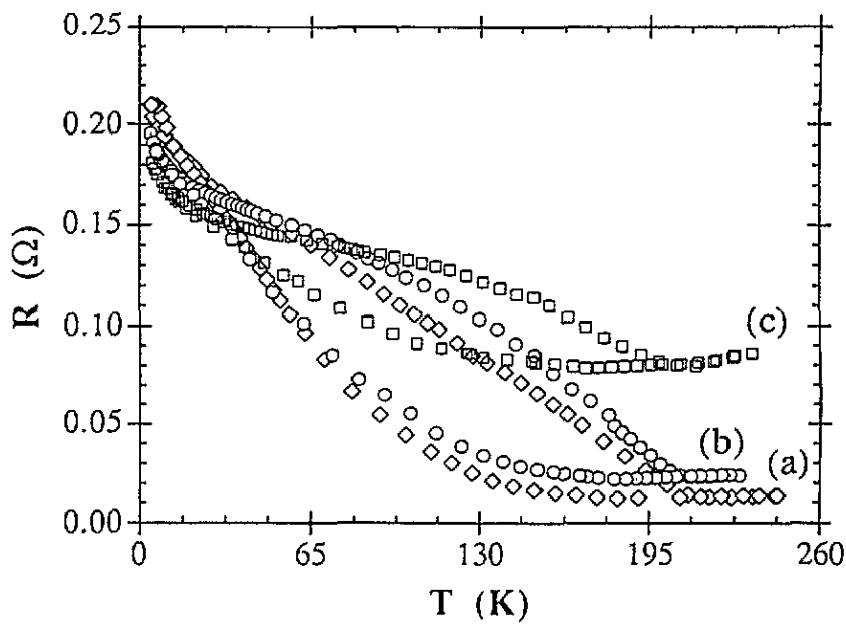

Figure 3. Resistivity measurements of the samples: data a, ◊, sintered at 923 K for 10 d and at 1023 K for 1 d; data b, ○, sintered at 923 K for 10 d; data c, □, sintered at 923 K for 1 d.

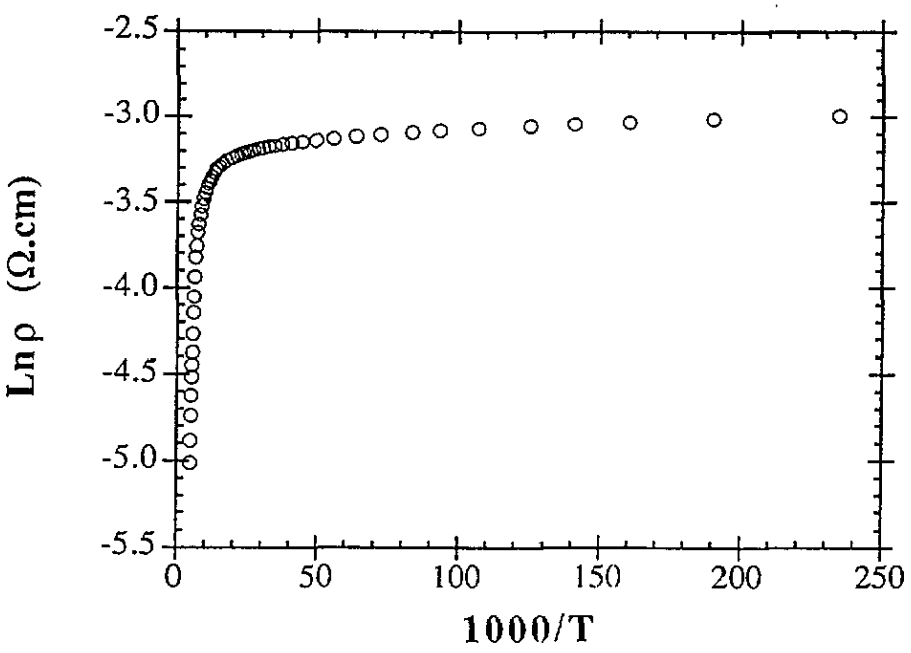

Figure 4. ln ρ versus $1000/T$ for a $NdNiO_{3-\delta}$ ceramic sample heated from 4.2 K to the metal–insulator transtion (about 205 K).

data were fitted to the expression for the VRH mechanism [20]:

$$\sigma = \sigma_0 \exp\left[-\left(\frac{T_0}{T}\right)^{1/4}\right]. \tag{1}$$

The constants σ_0 and T_0 in equation (1) are expressed functionally as [20]

$$\sigma_0 = e^2 a^2 \nu_{ph} N(E_F) \tag{2}$$

and

$$T_0 = \lambda\alpha^3/k_B N(E_F) \tag{3}$$

where e is the electronic charge, a is the hopping distance, ν_{ph} is a phonon frequency associated with the hop (calculated from the Debye temperature, it is around 10^{13} s^{-1}) and $N(E_F)$ is the density of states at the Fermi level. $\lambda(\approx 18.1)$ is a dimensionless constant, k_B is Boltzmann's constant and α is the inverse rate of fall-off of the wavefunctions associated with the localized states. The hopping distance depends slightly on the temperature following the expression

$$a = [\tfrac{9}{8}\pi\alpha k_B T N(E_F)]^{1/4}. \tag{4}$$

So the factor σ_0 also depends slightly on the temperature. A logarithmic plot of $\sigma T^{1/2}$ versus $1/T^{1/4}$ allows an accurate data analysis to be performed.

The logarithmic plot of $\sigma T^{1/2}$ versus $T^{1/4}$ and the best fit to equation (1) for sample a are shown in figure 5. As is observed, the logarithm of $\sigma T^{1/2}$ is linear with $T^{1/4}$ in the temperature range between 4.2 and 60 K approximately, indicating that the conduction mechanism in this interval is VRH of the carriers. The slight deviation at low temperatures (high values of $1/T^{1/4}$ in figure 5) could be due to electron–electron interactions [21] or maybe to the $\sigma_0 \propto T^{-1/4}$ dependence following the percolation theory of hopping for localized electrons with isotropic wavefunctions [22]. The best-fit values obtained for $\sigma_0 T^{1/2}$ and T_0 are $1.55 \times 10^3\ \Omega^{-1}\ \text{cm}^{-1}\ \text{K}^{1/2}$ and 1.1×10^3 K, respectively, and similar values were obtained by fitting the resistivity curve of sample b. With these results and making use of equations (2) and (3) the estimated values for $N(E_F)$ and α are $2.3 \times 10^{20}\ \text{eV}^{-1}\ \text{cm}^{-3}$ and $1.2 \times 10^6\ \text{cm}^{-1}$. The value of $N(E_F)$ is about two orders of magnitude lower than that reported by several workers [23, 24] for $LaNiO_3$. This result could be ascribed to the charge-transfer gap opening at lower temperatures than magnetic ordering of Ni ions or it could be correlated with the number of impurity states in the middle of the gap. As we have pointed out, the VRH mechanism is characteristic of impurity conduction in semiconductors or systems with small-polaron formation.

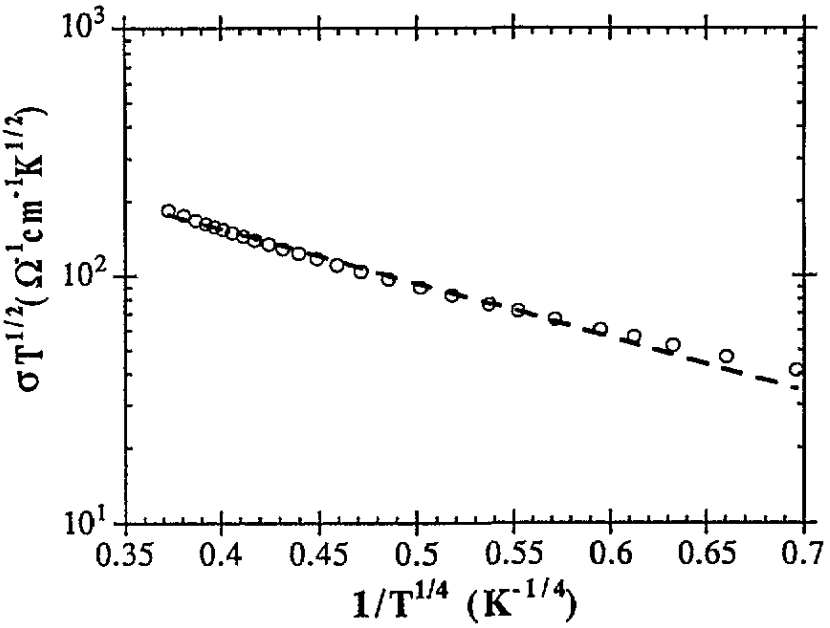

Figure 5. Semilogarithmic plot of $\sigma T^{1/2}$ versus $T^{-1/4}$ and the fit to equation (1) for a $NdNiO_{3-\delta}$ sample.

As can be seen in figure 6, the electrical behaviour for $NdNiO_3$ in the metallic phase shows a linear temperature dependence with $(1/\rho)(d\rho/dT) \simeq 1.5 \times 10^{-3}$. Similar values have been also reported for $LaNiO_3$, $PrNiO_3$ and high-temperature superconductors in the normal phase [23–25]. Some workers [19] have explained such behaviour in the framework of spin-polaron formation where the motion is a diffusive process following the Einstein equation

$$\sigma = ne^2 D/T \tag{5}$$

where n is the number of carriers, e is the electron charge and D is the diffusion coefficient. It has been suggested that, in systems in which the current transport is performed by spin polarons, the diffusion coefficient is temperature independent, resulting in a linear variation in the resistivity with temperature [19].

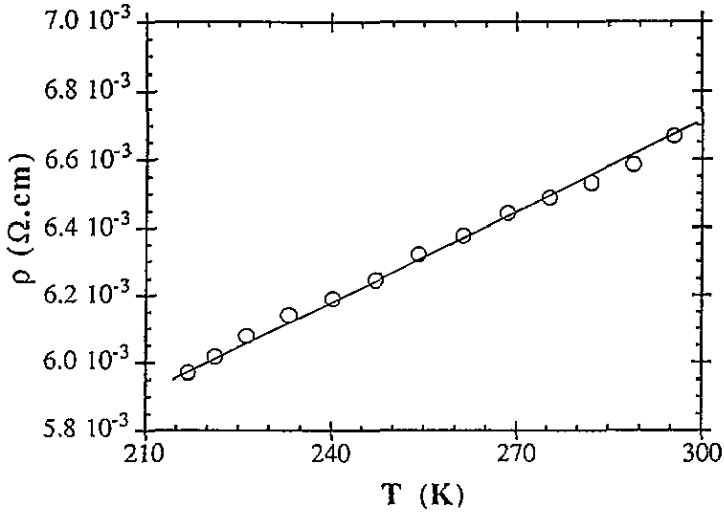

Figure 6. ρ versus T for a $NdNiO_{3-\delta}$ ceramic sample showing a linear dependence.

3.3. Magnetic properties

The AC magnetic susceptibility measurements between 1.7 and 300 K performed on different samples lead to the same values, independently of the sintering times. The $\chi(T)$ curve for sample a is reported in figure 7 and shows a Curie–Weiss-like paramagnetic behaviour. The inverse susceptibility as a function of temperature is a straight line from 100 to 300 K. Below this temperature the curve separates from this line, indicating the effect of the crystal-field splitting of the $J = \frac{9}{2}$ ground state of the Nd^{3+} free ion. The sudden increase in the susceptibility at very low temperatures may be due to the polarization of Nd^{3+}, but no kind of rare-earth ordering was detected down to 1.7 K.

At room temperature the susceptibility is 2.186×10^{-5} emu g^{-1}, in agreement with previous results [6]. At relatively high temperatures the data in figure 3 have been fitted to the law

$$\chi = \frac{C}{T - \Theta} + \chi_0. \tag{6}$$

This is the sum of a Curie–Weiss function and a temperature-independent χ_0 term, which takes into account the Pauli paramagnetism, the Van Vleck paramagnetism and the ion core diamagnetism. This fit gives the values of $C = 6.38 \times 10^{-3}$ emu K g^{-1}, $\Theta = -53.3$ K and $\chi_0 = 3.87 \times 10^{-6}$ emu g^{-1}. The effective magnetic moment μ_{ef} calculated is $3.57\mu_B$ (μ_B is the Bohr magneton). This value is very close to the theoretical moment expected for a free Nd^{3+} ion of $3.62\mu_B$. The temperature-independent contribution χ_0 is due mainly to the Pauli paramagnetism of itinerant electrons and its value is similar to that reported for

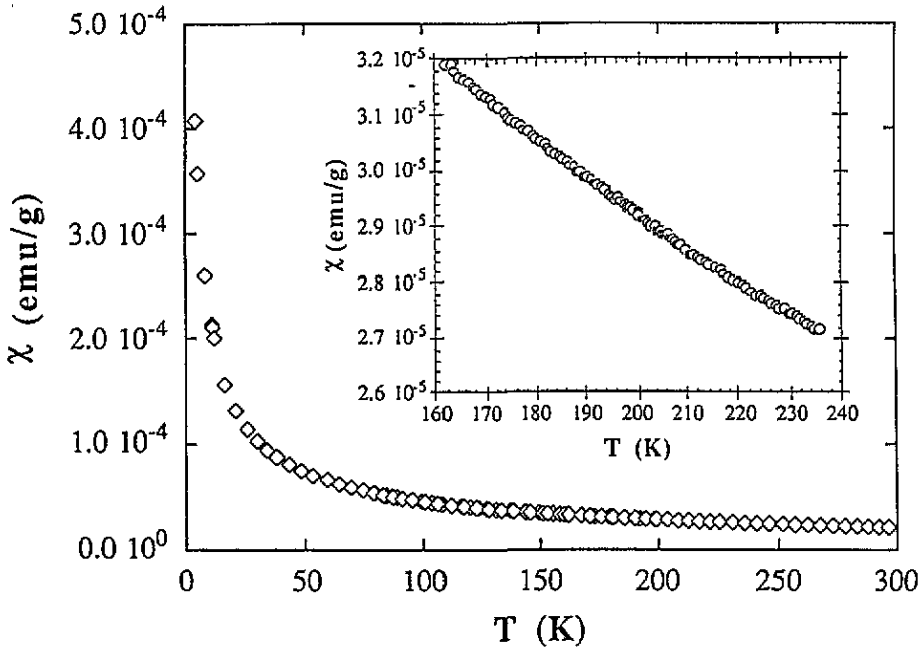

Figure 7. Magnetic susceptibility versus temperature for $NdNiO_{3-\delta}$. The inset shows, in detail, the susceptibility curve in the proximity of the metal–insulator transition.

$LaNiO_3$ [24–26]. If we take as $NdNiO_3$ core diamagnetism the value calculated from similar systems, such as $LaNiO_3$ and $PrNiO_3$ [25] (68×10^{-6} emu mol^{-1}), the Pauli paramagnetism can be estimated as 9.5×10^{-4} emu mol^{-1}. From this value, the calculated band-structure density of electron states at the Fermi level, using the relation $\chi^{Pauli} = \mu_B^2 N(E_F)$, is around 7.25×10^{22} eV^{-1} cm^{-3}. It is significantly high with respect to band-structure calculations [27] but it is in agreement with recent results reported in correlated systems [23–25].

An important result is the absence of any magnetic anomaly at the metal–semiconductor transition can be seen in the inset of figure 7. In this range of temperatures, the measurement was carried out carefully with increasing steps of 0.5 K, and no anomaly was observed in $\chi(T)$ nor in its derivative. This result agrees with most data reported for HT-$NdNiO_3$ with the exception of a light anomaly in the derivative data reported recently [9].

The lack of magnetic contribution from the Ni sublattice and the absence of any anomaly in $\chi(T)$ at the transition temperature are obscure points which should be solved. Some workers have suggested a negligible discontinuity due to the simultaneous electronic localization and Ni^{3+} antiferromagnetic ordering [1,7]; it could be hidden by the strong Nd^{3+} paramagnetism [7].

In order to determine whether the high increase in the susceptibility at low temperatures is associated with some ferromagnetic component, DC magnetization was measured at 1.7 and 4.2 K for external magnetic fields up to 5 T. Both measurements are characteristic of paramagnetic behaviour following a Brillouin curve. Moreover, the absence of magnetic remanence and magnetic hysteresis indicate the absence of ferromagnetic contributions and the increase in $\chi(T)$ would be due to polarization of the rare-earth sublattice. As has been reported, the Ni^{3+} ($S = \frac{1}{2}$) sublattice order in HT-$NdNiO_3$ implies ferromagnetic and antiferromagnetic interactions [11]. Because of this particular arrangement of the Ni

spins, the exchange field is non-zero in half the Nd^{3+} ions and zero in the other half [28]. The internal field can polarize half the Nd ions, explaining the increase in the magnetic susceptibility at low temperatures.

3.4. Heat capacity

Heat capacity measurements in a heating run from 4.2 to 300 K of a $NdNiO_3$ sample are shown in figure 8. A scaling value of $C_p/R = 12.46$ at $T = 270.15$ K determined from DSC measurements was used. The low-temperature heat capacity shows an upturn starting at 10 K down to 4.2 K corresponding to the Schottky-like contribution from the ground-state level of Nd^{3+} [29]. A second anomaly is observed in the heating run at the temperature of the insulator–metal transition ($T = 185$ K) characterized by a small hump of about 2% of the total heat capacity. The heating and cooling experiments near the metal–insulator transition are compared in figure 9. The cooling $C_p(T)$ curve does not show any anomaly at this temperature and crosses the $C_p(T)$ heating curve at 140 K. This behaviour is in agreement with the large hysteresis observed in the electrical resistivity study. In fact, the lack of anomaly confirms the continuous transition from the metallic to the semiconducting phase.

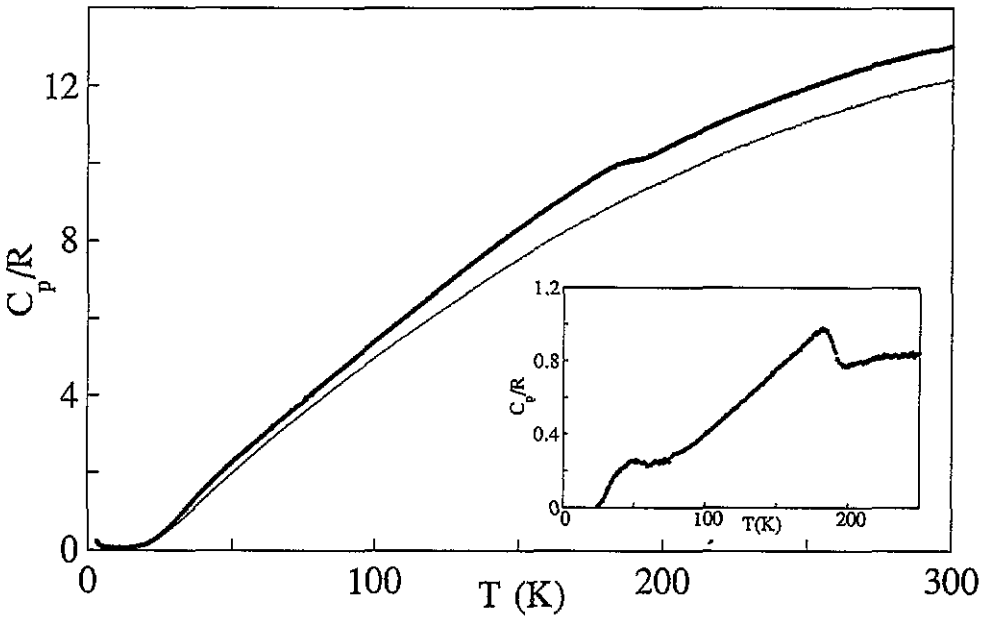

Figure 8. Heat capacity of $NdNiO_3$ (●) and $NdGaO_3$ (·). $NdGaO_3$ has been scaled in temperature by applying the corresponding states law. The inset shows the excess heat capacity due to the magnetic and electronic contribution after subtracting the estimated baseline with the scaled $NdGaO_3$.

In order to evaluate the electronic and nickel's magnetic contributions to the heat capacity and, in particular, to estimate the entropy change at the metal–insulator transition, we have measured the insulating compound $NdGaO_3$. This compound presents the same crystallographic structure as $NdNiO_3$ and a similar crystal-field splitting of the Nd^{3+} levels is expected. With this consideration, we assume that the lattice heat capacity and the

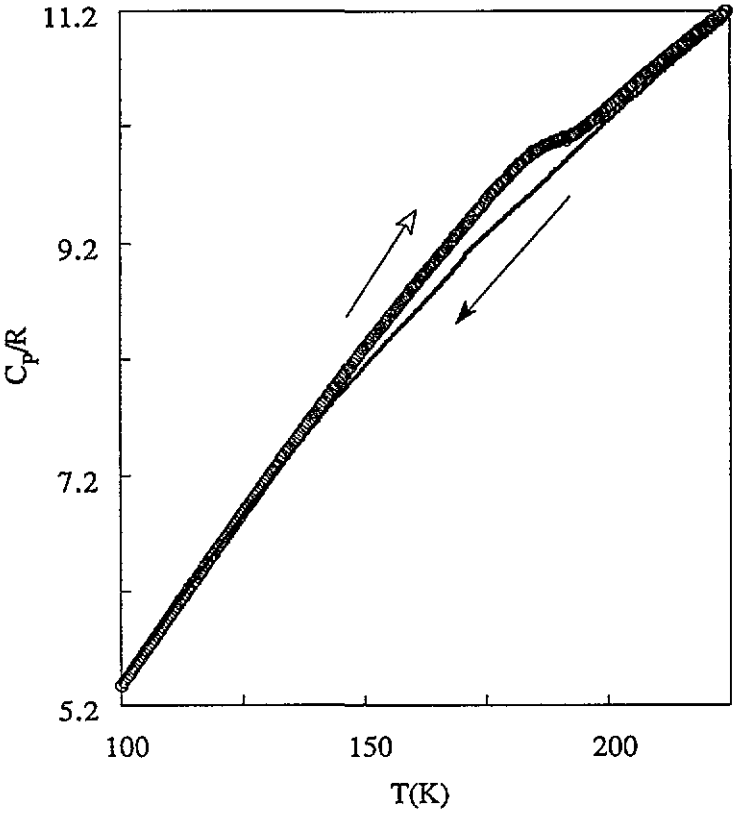

Figure 9. $NdNiO_3$ heat capacity near the metal–insulator transition. Measurements were obtained on a heating run (O) and on a cooling run (·).

contribution from the depopulation crystal-field levels of Nd^{3+} in $NdNiO_3$ can be obtained using the heat capacity of $NdGaO_3$ after applying the corresponding states law. The comparison between the measured heat capacities of $NdNiO_3$ and $NdGaO_3$ scaled in temperature by a factor of 1.036 (obtained using the Lindemann relation [30]) is shown in figure 8. The difference between these two curves, plotted in the inset of figure 8, corresponds to the sublattice nickel magnetic contribution and the electronic contribution. At high temperatures, i.e. in the metallic phase, the high anomalous heat capacity value can be due to the strong correlations with phonons, leading to a large electronic contribution. Taking into account the difficulty of estimating the entropy associated with the phase transition, we have calculated the limits for this value. We obtain the total entropy contribution $\Delta S(280\ \mathrm{K}) = 1.04R$ and $\Delta S(200\ \mathrm{K}) = 0.76R$, by integration of the residual C_p/T between 25 and 280 K and between 25 and 200 K. This last value includes the gain in entropy in the electronic delocalization process added to the gain from the spin disorder of the localized Ni^{3+} magnetic moments. From the electronic heat capacity coefficient obtained from the low-heat-capacity measurement of $LaNiO_3$ [23, 31], $\gamma = 13$–15 mJ mol^{-1} K^{-2} we have estimated the contribution ascribed to the electronic localization, $\Delta S_{elec}(200\ \mathrm{K}) = \gamma 200\ \mathrm{K} = (0.31\text{–}0.36)R$, so that the magnetic entropy below the transition temperature will be $\Delta S_{mag} = (0.45\text{–}0.40)R$. This value is lower than the theoretical value of $R\ln 2 = 0.69R$, corresponding to an $S = \frac{1}{2}$ spin ordering. This analysis shows that some ordering of the nickel magnetic moments are associated with the phase transition but the

entropy value is lower than the expected one. This can indicate some magnetic correlations above the transition temperature. This can also explain the excess in the heat capacity from the γT electronic value, using the $LaNiO_3$ data, above 200 K.

Looking at the inset of figure 8, we observe the presence of a small jump with the maximum at 50 K in the residual heat capacity. This anomaly could be due to the change in the behaviour of the carriers passing from the VRH regime to the semiconducting regime. The similar temperatures for the heat capacity anomaly and start point for the VRH mechanism can be noted. Other possible explanations could be connected with small differences in the multiplet splitting of the Nd^{3+} ion between $NdNiO_3$ and $NdGaO_3$.

4. Discussion and conclusions

We would like to emphasize several aspects of the present study. The $NdNiO_3$ sample can be prepared at low temperatures and low oxygen pressures by means of a sol–gel method. This method yields an oxygen-deficient perovskite of nominal composition $NdNiO_{2.91}$ with a degree of crystallization depending essentially on the sintering time.

The crystallographic study has shown that $NdNiO_{2.91}$ is orthorhombic as is the compound prepared at high oxygen pressures. The main difference observed in the diffraction patterns is the presence of anomalous asymmetric reflections which are explained by the presence of laminar disorder that could be associated with the lack of oxygen stoichiometry.

The resistivity curve shows, as in the case of the HT-$NdNiO_3$, a metal–insulator transition and the most important difference is the large thermal hysteresis of our material. All the samples prepared with different grain sizes show essentially the same behaviour in their electrical transport properties, guaranteeing the intrinsic behaviour of the material. The analysis of the resistivity curve demonstrates that the conductivity mechanism cannot be explained either as in a classical semiconductor with a fixed activation energy in the low-temperature phase or by the motion of electrons in a conduction band in the metallic phase. Because of the absence of exhaustive studies on the electronic properties of HT-$NdNiO_3$ at low temperatures, we cannot be sure whether our results are a general feature or whether they are associated with the lack of oxygen stoichiometry.

The previous works on the semiconductor–metal transition of $RENiO_3$ describes these compounds as charge-transfer insulators at low temperatures, the transition originating from the closing of the band-transfer gap. This gap is controlled by coupled tilts of NiO_6 octahedra, which imply changes in the Ni–O–Ni angle. This angle controls the transfer integral between Ni e_g^* and O 2p orbitals. This mechanism is in agreement with the macroscopic phenomenology of the $RENiO_3$ systems and qualitatively explains the relationship between the O–Ni–O angle and the phase transition temperature in this family [1, 6]. Moreover, it has been reported, from neutron diffraction results, that simultaneous electronic localization and antiferromagnetic ordering of the $S = \frac{1}{2}$ Ni sublattice occur, giving a spin wave with an ordering not previously described in perovskite oxides [11].

As has been pointed out in the previous section, the analysis of the electrical resistivity shows that the activation energy varies strongly with the temperature, giving a behaviour similar to that of NiO doped with Li. Resistivity measurements reported on HT-$NdNiO_3$ at low temperatures also show a temperature-dependent activation energy [9]. We have shown that the conduction mechanism at low temperatures in the semiconducting phase follows a VRH mechanism while in the metallic phase the motion is diffusive. This indicates a large electronic correlation in this material in the high-temperature and in the low-temperature phases, in agreement with recent results [23–25]. A possible explanation is that the carriers

in these systems could be formed by the coupling of electrons with phonons or magnons, i.e. polarons or spin polarons. Although the analysis of the low-temperature resistivity data leads to a reasonable value of the density $N(E_F)$ of states at the Fermi level, the radius of the polaron is so high ($R = 80$ Å) that it makes small-polaron formation impossible. Nevertheless, several workers have indicated that spin polarons are large polarons and their motion in magnetic semiconductors may be similar to the usual small-polaron motion [32]. On the other hand, the thermopower measurements of $PrNiO_3$ recently reported show a maximum value at 55 K, probably indicating impurity states in the gap [24] characteristic of impurity conduction. Further work is in progress in order to clarify this important point.

Anyway, the possible formation of spin polarons is also supported by the study of the magnetic susceptibility. This oxide shows a Pauli susceptibility ($\chi_p \simeq 9.15 \times 10^{-4}$ emu mol^{-1}) which is abnormally high and similar to that reported for $LaNiO_3$ or $PrNiO_3$ [23–26]. This anomalous high temperature-independent paramagnetism has been interpreted in the framework of a highly correlated gas of ferromagnetically coupled spin polarons [26]. Moreover, the absence of anomaly in the $\chi(T)$ curve at the metal–insulator transition is very significant and does not correspond to the discontinuity observed in other oxides, such as V_2O_3 [5], where the spin localization induces a sharp discontinuity of the susceptibility curve, or the usual anomaly observed in the antiferromagnetic ordering of localized spins. Some workers claim that the coincidence of both transitions (magnetic and electrical) can explain the absence of a magnetic contribution for this compound and for related $PrNiO_3$ [2, 7]. The lack of anomaly could be explained in another way by supposing that there are some kinds of spin correlation in the high-temperature phase, suggesting (as do the resistivity measurements) spin-polaron formation.

The calorimetric study also supports spin correlation in the high-temperature phase. In fact, the magnetic and electronic entropy estimated for the metal–insulator transition is lower than expected for the ordering of an $S = \frac{1}{2}$ lattice and the contribution to the high-temperature phase of the heat capacity seems to indicate that some magnetic contribution would be present.

In summary, the heat capacity, magnetic susceptibility and electrical resistivity data indicate that spin correlation exists in the high-temperature phase and that the charge carriers would behave as polarons. New measurements of the transport properties such as the frequency dependence of the AC conductivity, Hall effect and magnetoresistance are in progress in order to corroborate the proposed hypothesis.

Acknowledgments

This work was supported by CICYT under grants MAT 93-0240-C04-04, MAT 91-0923-c02-01 and PB92-1077. The authors express their thanks to Dr J Bartolomé and F Bartolomé for fruitful discussions.

References

[1] García-Muñoz J L, Rodríguez-Carvajal J, Lacorre P and Torrance J B 1992 *Phys. Rev.* B **46** 4414
[2] Lacorre P, Torrance J B, Pannetier J, Nazzal A I, Wang P W and Huang T C 1991 *J. Solid State Chem.* **91** 225
[3] Huang T C, Parrish W, Toroya H, Lacorre P and Torrance J B 1990 *Mater. Res. Bull.* **25** 1091
[4] Demazeau G, Marbeauf A, Pouchard M and Hagenmuller P 1971 *J. Solid State Chem.* **3** 582
[5] Tsuda N, Nasu K, Yanase A and Siratori K 1991 *Electronic Conduction in Oxides* (Berlin: Springer)

[6] Torrance J B, Lacorre P, Nazzal A I, Ansaldo E J and Niedermayer Ch 1992 *Phys. Rev.* B **45** 8209
[7] Vassiliou J K, Hornsbostel M, Ziebarth R and Disalvo F J 1989 *J. Solid State Chem.* **81** 208
[8] Blasco J, García J, Proietti M G and Chaboy J 1993 *Solid State Ion.* **63–65** 585
[9] Canfield P C, Thompson J D, Cheong S-W and Rupp L W 1993 *Phys. Rev.* B **47** 12357
[10] Granados X, Fontcuberta J, Obradors X and Torrance J B 1992 *Phys. Rev.* B **46** 15683
Obradors X, Paulius L M, Maple M B, Torrance J B, Nazzal A I, Fontcuberta J and Granados X 1993 *Phys. Rev.* B **47** 12353
Granados X, Fontcuberta J, Obradors X, Mañosa Ll and Torrance J B 1993 *Phys. Rev.* B **48** 11666
[11] García-Muñoz J L, Rodríguez-Carvajal J and Lacorre P 1992 *Europhys. Lett.* **20** 241
[12] Medarde M, Fontaine A, García-Muñoz J L, Rodríguez-Carvajal J, de Santis M, Sacchi M, Rossi G and Lacorre P 1992 *Phys. Rev.* B **46** 14975
[13] Kuiper P, Kruizinga G, Ghijsen J and Sawatzky G A 1989 *Phys. Rev. Lett.* **62** 221
[14] García J, Blasco J, Proietti M G and Benfatto M 1994 *XAFs VIII Conference (Berlin)* at press
[15] Rillo C, Lera F, Badía A, Angurel L A, Bartolomé J, Palacio F, Navarro R and van Duyneveldt A J 1991 *Magnetic Susceptibility of Superconductors and Other Spin Systems* (New York: Plenum) pp 1–24
[16] Rodriguez J, Anne M and Pannetier J 1987 *Institut Laue–Langevin Report* 87TR014T
[17] Warren B F and Bodenstein P 1966 *Acta Crystallogr.* **20** 602
[18] Springthorpe A J, Austin I G and Austin B A 1965 *Solid State Commun.* **3** 143
[19] See for example Mott N F 1990 *Metal–Insulator Transitions* (London: Taylor & Francis)
Mott N F and Davis E A 1979 *Electronic Processes in Non-crystalline Materials* (Oxford: Oxford University Press)
[20] Paul D K and Mitra S S 1973 *Phys. Rev. Lett.* **31** 1000
[21] Efros A L and Shklovskii B I 1975 *J. Phys. C: Solid State Phys.* **8** L49
Ionov A N, Matveev M N, Rentch R and Shlimak I S 1985 *JETP Lett.* **42** 406
[22] Shklovskii B I and Efros A L 1984 *Electronic Properties in Doped Semiconductors* (Berlin: Springer)
[23] Rajeev K P, Shivashankar G V and Raychaudhur A K 1991 *Solid State Commun.* **79** 591
[24] Xu X Q, Peng J L, Li Z Y, Ju H L and Greene R L 1993 *Phys. Rev.* B **48** 1112
[25] Sreedhar K, Honig J M, Darwin M, McElfresh M, Shand P M, Xu J, Crooker B C and Spalek J 1992 *Phys. Rev.* B **46** 6328
[26] Goodenough J B 1971 *Prog. Solid State Chem.* **5** 276
[27] Kemp J P and Cox P A 1990 *Solid State Commun.* **75** 731
[28] Medarde M, Rosenkranz S, Fischer P, Furrer A and Lacorre P 1993 *Proc. Euroconf. on Dynamic Properties of Condensed Matter (Patras, 21–26 September, 1993)*
[29] Bartolomé F and Bartolomé J 1994 *Solid State Commun.* at press
[30] Lindemann F 1910 *Z. Phys.* **11** 609
[31] Sánchez R D, Causa M T, Sereni J, Vallet-Regí M, Sayagués M J and González-Calbet J M 1993 *J. Alloys Compounds* **191** 287
[32] See for example von Malnar S and Methfessel S 1967 *J. Appl. Phys.* **38** 959
Kasuya T, Yanese A and Takeda T 1970 *Solid State Commun.* **8** 1551